# Ethanol on graphite: Ordered structures and delicate balance of interfacial and intermolecular forces

Xing He, Ding-Shyue Yang\*

Department of Chemistry, University of Houston, Houston, Texas 77204 United States

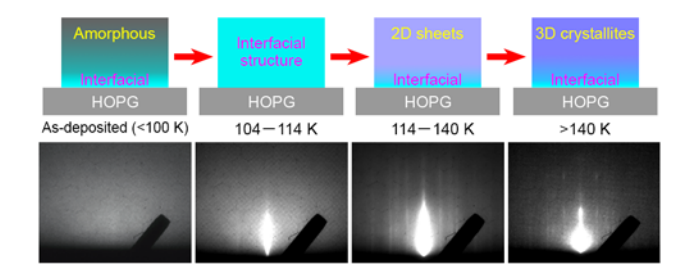
<sup>\*</sup>To whom correspondence should be addressed. Email: yang@uh.edu

#### **Abstract**

Clear knowledge of solid-molecule interfacial structures is essential to the understanding of interfacial phenomena and the interplay of surface effects and intermolecular forces. Molecules that can form hydrogen bonds are of particular interest. Here, we report the structures and phasetransition behavior of (sub)nanometer-thick ethanol assemblies deposited on highly orientated pyrolytic graphite. Depending on the film thickness and temperature, three ordered structures of ethanol are observed: first, an interfacial one formed after deposition at ~100 K that is nearcommensurate with the supporting graphene lattice, up to a nominal thickness of 1.5 nm; second, stacking of two-dimensional layered sheets at  $\geq 114$  K for the upper part of thicker films of  $\sim 2$ nm and above; and third, a monoclinic bulk-like structure appearing at ~144 K before desorption. Importantly, the whole amorphous-to-crystalline transition undergoes a complex multi-step process, with the extension of the interfacial structure reaching much further away from the substrate surface and then being replaced within a low-temperature range. Together with the lattice strain found in the interfacial assembly, these thickness- and temperature-dependent structures and transition behavior signify a delicate balance between all interfacial and intermolecular forces involved and molecular free energy.

**Keywords**: Layered materials, van der Waals interactions, reflection high-energy electron diffraction, epitaxial growth, terraced surface topography

**TOC Graphic** 



## 1. Introduction

It is known that structures at interfaces where different materials and/or molecules meet have fundamental impacts on materials properties and behavior, interfacial phenomena, and even device performance in practical applications. 1-5 For small molecules, especially those capable of forming hydrogen bonds such as water, methanol, ethanol, etc., knowledge of their interfacial structures has particular importance due to their broad existence as common solvents and in fuel cells, catalysis, macromolecular systems, and interstellar matter. <sup>6-12</sup> Given the relatively large strength and directional nature among intermolecular forces, hydrogen bonds play an important role in the organization of assembly structures, which may be in competition or sometimes cooperation with substrate-molecule interactions. Hence, to reveal interfacial structural details as a result of a delicate balance of all forces involved, it is crucial to use structure-probing techniques with suitable surface sensitivity, e.g., scanning probe microscopy, 13-14 reflectionabsorption infrared spectroscopy, <sup>15-17</sup> and reflection diffraction methods. <sup>18-20</sup> In recent years, reflection high-energy electron diffraction (RHEED) has been used to elucidate unanticipated ordered assemblies and unusual phase-transformation behavior of small molecules physisorbed or chemisorbed on different surfaces. 21-30 The technique's strengths of a (sub)nanometer-thick penetration depth at grazing incidence angles and resulting surface sensitivity make noncontacting RHEED highly suitable for temperature- and thickness-dependent studies of interfacial structures and phase transitions of molecular systems, beside its typical use during thin-film fabrications in materials science.

Several factors may affect the structures of molecular films deposited on a supporting substrate, including the interplay of interfacial and intermolecular interactions, <sup>26, 31</sup> temperature<sup>21, 24</sup> and molecular free energy, <sup>32</sup> deposition rate, <sup>33-35</sup> and the degree of lattice matching. <sup>36-37</sup> For

the latter, both in-plane epitaxy and out-of-plane topographical template effects may be important, especially for situations without covalent-type bonding as a guiding force. The in-plane epitaxial relation between a molecular overlayer structure and the substrate lattice can be categorized into the commensurate, coincident, and incommensurate types. 36-37 If good lattice matching such as a commensurate epitaxy exists, an ordered molecular overlayer may likely form in a specific azimuthal orientation with respect to the surface. However, such an interfacial structure is often different from those observed in the bulk, even if polymorph phases exist. As a result, how an interfacial order transitions into a bulk-like structure in the upper part of a multilayer film away from the supporting solid becomes a complex problem and may be crucial to the understanding of molecular behaviors at interfaces. 12, 17, 21-22, 38-39

Ethanol is known for the presence of different solid forms depending on the temperature and thermal process used. For the bulk, rapid cooling to a temperature lower than 100 K results in an amorphous solid, whereas a rotator phase and an orientational glass may be produced by moderate cooling of the liquid. The monoclinic crystalline structure can be readily obtained at a temperature close to melting or by annealing of the amorphous solid. Above a solid surface, ethanol molecules have been reported to form commensurate overlayer structures on gold<sup>44</sup> and graphite (with high mosaic-angle disorder). However, a detailed study of the structural and phase-transition evolution of ultrathin to multilayer ethanol films (transitioning from an interfacial structure to the bulk one) on highly-ordered graphite is still lacking and thus needs further investigation.

In this report, RHEED is used to directly resolve the assembly structures in vapordeposited ethanol films with a thickness of sub-monolayer to multilayers up to more than 10 nm. The analysis of the near-commensurate interfacial structure and its lattice strain observed in nominally <1.5-nm films provide key information for the question about the "interfacial region." Above it, the bulk-like monoclinic structure is found in the upper part of thicker films during thermal annealing to higher temperatures. However, the formation does not proceed in a single amorphous-to-crystalline step as conventionally considered. Instead, in-plane two-dimensional (2D) sheets containing puckered hydrogen-bonded (HB) chains are produced first without a long-range cross-plane order, followed by the final appearance of three-dimensional (3D) ordered, not randomly oriented, crystallites in a small temperature range close to molecular desorption. More surprisingly, the interfacial structure can extend more than 10 nm away from the graphite surface and then withdraw within a low-temperature range, which implies a dynamic behavior of the structural transition. These fruitful observations signify a delicate balance of interfacial and intermolecular forces involved as well as molecular free energy.

# 2. Experimental Section

Highly oriented pyrolytic graphite (HOPG, ZYA grade) used for ethanol depositions was purchased from SPI Supplies., with a mosaic spread angle of  $0.4^{\circ}\pm0.1^{\circ}$ . Immediately before its loading into the vacuum chamber assembly, a fresh surface of the HOPG substrate was produced by Scotch-tape cleavage and then clamped onto a flag-style sample holder plate for good thermal contact. A K-type thermocouple with an accuracy of <1 K was attached to the HOPG substrate for direct measurement of the surface temperature. The procedure for molecular depositions has been described in a previous report. Briefly, anhydrous ethanol (200 proof, molecular biology grade) was purchased from Decon Labs and used without further purification. The pure alcohol was loaded into a stainless-steel reservoir in a nitrogen-filled glovebox and then quickly connected to the home-built effusion-type molecular doser. After multiple freeze-pump-thaw cycles, purity of the effused ethanol vapor was further confirmed by the absence of other

molecular ion peaks, especially those associated with water, using a residual gas analyzer that is sensitive to a partial pressure of  $10^{-10}$  torr. The ultrahigh vacuum chamber for molecular depositions, annealing, and diffraction measurements had a base pressure of the level of  $10^{-10}$  torr, with the only discernible peaks in the mass spectra being from the hydrogen atomic and molecular species. To vapor-deposit thin films, the HOPG substrate was placed below the doser at a distance of a few centimeters. The deposition rate was in the range of 1–2 nm/min calibrated by an optical reflectance measurement. All depositions were made beginning with a bare HOPG surface and ended by closing a valve to stop the ethanol vapor. The nominal thickness was calculated from the controlled deposition time. Through the contact with a cryostat and an integrated heater, the substrate temperature can reach as low as 95 K using liquid nitrogen as the cryogen and be raised to a higher value for annealing, whose typical ramp rate was  $\sim 1.3$  K/min.

Reflection high-energy electron diffraction (RHEED) was used for direct probing of the structures of interfacial ethanol at different coverages and specimen temperatures. The kinetic energy of probing electrons was 30 keV, corresponding to a de Broglie wavelength of 0.07 Å. The diffraction patterns were recorded by an imaging assembly consisting of a phosphor screen fiber-coupled to an image intensifier and then a CMOS camera (Ander Zyla HF). The average flux of probe electrons was maintained at an extremely low level of the order of <1 pA/mm<sup>2</sup> (equivalently, an ultralow accumulated dose of less than 0.0005 e/Å<sup>2</sup> in 2 h), which we confirmed to have no effects or induced changes due to the electron impact or radiation damage within the measuring time (less than 2 hours). The probe depth of the RHEED measurements was estimated to be  $\sim1$  nm based on a trigonometric relation using the elastic mean free path of 30-keV electrons in an ethanol crystal, which is  $\sim107$  nm, and the typical angle of grazing incidence of  $\sim0.5^{\circ}$ .

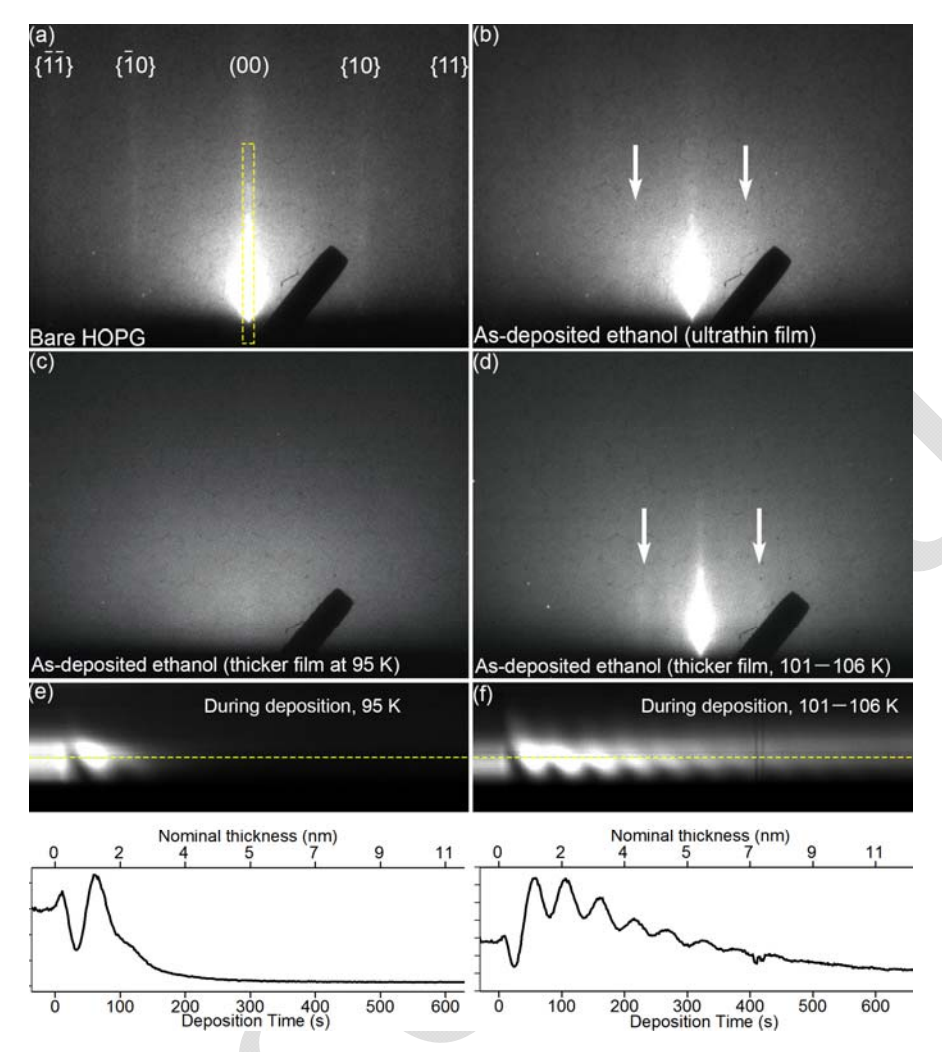


**Figure 1.** RHEED images and diffraction intensity changes as a function of ethanol coverage. (a) Diffraction pattern of bare HOPG before molecular deposition. The Miller indices for the diffraction streaks are labeled. The vertical strip enclosed in the yellow dashed rectangle is the region used for the analysis of intensity changes. (b) Diffraction pattern of an as-deposited ultrathin ethanol film with a nominal thickness of 0.4 nm. The arrows indicate the new diffraction features different from those weakened ones of HOPG. (c) and (d) RHEED patterns of 10-nm films deposited at 95 K and within the mildly elevated temperature range of 101–106 K, respectively. In these images, the shadow of the electron beam block to prevent oversaturation by the direct beam is seen as the tilted black rectangle. (e) and (f) Evolutions of the center streak intensity profile [derived from the yellow rectangular region in (a)] during deposition (as the horizontal axis) at the respective temperatures of (c) and (d). The curves in the lower panels of (e) and (f) are the intensity values indicated by the yellow dashed lines in the upper panels, as a function of deposition time. The corresponding nominal thicknesses are also given.

#### 3. Results and discussion

# 3.1 Deposition of ethanol nanoscale films on HOPG

Shown in Figure 1 are the RHEED images obtained before and after the depositions of ethanol ultrathin films on HOPG as well as the diffraction intensity changes as a function of coverage in two different temperature ranges. From the apparent differences, it is evident that both the substrate temperature and the film thickness influence the structure of an ethanol assembly on HOPG, which implies the important role of the relative strength of the graphite-ethanol and intermolecular interactions compared to the molecules' thermal energy. For an ultrathin film with a nominal thickness of 0.4 nm, ordering of ethanol molecules was immediately formed after their physisorption on HOPG even at a temperature as low as 95 K without annealing, as indicated by the new streaks different from those of HOPG (Figure 1, a and b). It will become clear in later discussion that the interfacial and intermolecular forces work in a cooperative fashion to form a HB chain structure that is commensurate to the basal plane of graphite and different from that of solid ethanol bulk. As the film thickness increases at 95 K, an amorphous film without an assembly order is resulted, giving a diffuse RHEED pattern without clear diffraction features (Figure 1c for 10 nm). This finding is generally anticipated in that interfacial ordering as a result of the graphene-ethanol interaction loses its influence after some distance, and therefore the ethanol molecules away from the interface are immobilized with various molecular orientations. However, if the growth temperature is raised to the range of 101–106 K, a streaky pattern similar to that from a sub-monolayer coverage is again observed, which signifies, surprisingly, the presence of a similarly ordered structure for as-deposited multilayer films (Figure 1d for 10 nm compared to Figure 1b). In fact, thicker films deposited at <100 K can also produce a similar RHEED pattern as shown Figure 1e if gently warmed by a few degrees.

Thus, such significant behavioral differences found with a small change of the substrate temperature strongly suggest a delicate balance of all the interactions involved and thermal energy, which critically affects the structural organizations nearby and away from the solid—molecule interface.

The diffraction intensity variation as a function of deposited coverage further shows the distinct difference in the film growth at different temperatures. It is known that RHEED is frequently used as an in situ technique to monitor surface structures and morphology during the growth of solid thin films. Maxima of diffraction intensities as a function of deposition time indicate the completion of an atomic or molecular layer, whereas local minima correspond to the surface condition of high roughness for incomplete layers causing more diffuse scattering.<sup>47</sup> Here, we find that at 95 K, only 2–3 intensity maxima are discernible, which signifies the limited thickness range for the ordered interfacial structure and likely the lack of a layer-by-layer growth in thicker films (Figure 1e). In contrast, a periodic modulation during deposition at a slightly elevated temperature is clearly seen in Figure 1f for an extended thickness range, indicating the transition to a layer-by-layer (or, at least, Stranski-Krastanov<sup>48</sup>) growth mode adopting the interfacial structure with order in upper layers; each "effective" layer is ~1.0 nm thick as indicated by the oscillatory RHEED intensity shown in Figure 1f, which should contain more than one ethanol sheet considering the usual van der Waals distances. Such an observation also signifies the production of a smooth film and a low tendency for growth of 3D islands (at least in the range of several nm) that was seen in other graphite-particle systems. 38, 49 Thus, these results provide, from a structural viewpoint, a look at the differences in the molecular orientations (see below) and hence wetting at the interface in these temperature ranges. Based on a quick estimate considering the modes of molecular motions and forces involved between molecules, a low value of several kJ/mole might be the activation energy to convert an amorphous overlayer with high free energy content to a more ordered interfacial structure with lower energy.

## 3.2 Monoclinic phase of solid ethanol

Thermal annealing of a nanoscale ethanol film thicker than 2 nm above 120 K leads to its gradual transition to a crystalline phase. However, instead of forming randomly oriented crystallites, which would produce a RHEED image with Debye–Scherrer rings, the diffraction streak pattern shown in Figure 2a indicates a high degree of order with an in-plane 2D nature in the assembly structure. Moreover, the phase transition does not proceed in a single stage; only at a temperature above 140 K, just a few degrees before complete sublimation of a deposited film, do the diffraction streaks begin evolving into more defined spots with slightly narrowed horizontal widths, although the vertical widths are still apparently larger than typical values from 3D-ordered solids (Figure 2c). Using the Scherrer formula, <sup>50</sup> we estimate that the average sizes

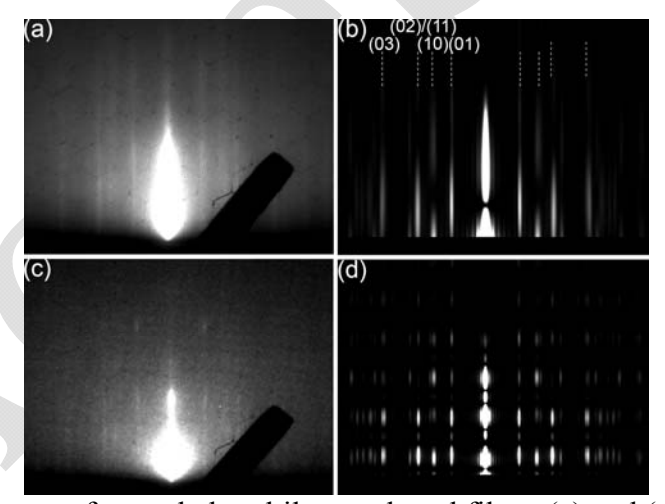


**Figure 2.** RHEED patterns of annealed multilayer ethanol films. (a) and (c) Experimental images of 10-nm films acquired at  $\sim$ 140 K and  $\sim$ 147 K, respectively. (b) Simulated pattern obtained using a crystalline domain of  $10\times1\times10$  unit cells (i.e.,  $5.4\times0.7\times8.3$  nm<sup>3</sup> with the lateral size roughly matching the experimentally determined average value). The 2D Miller indices for different streaks are assigned. (d) Simulated pattern obtained using a crystalline domain of  $17\times3\times17$  unit cells (i.e.,  $9.1\times2.1\times14.0$  nm<sup>3</sup> with increased lateral and vertical sizes approximately matching the enlarged average values reported in the text).

of these two structures are 7.3 nm for the 2D-layered domains in Figure 2a and 12.5 nm laterally and 2.2 nm vertically for the crystalline slabs in Figure 2c.

According to previous reports, solid ethanol has a monoclinic crystal structure (a = 5.377 Å, b = 6.882 Å, c = 8.255 Å, and  $\beta = 102.2^{\circ}$ ) in this elevated temperature range.<sup>42,51</sup> To index the observed RHEED pattern, theoretical simulations based on kinematic scattering theory<sup>22</sup> were performed using the monoclinic crystal structure. An agreement is found when the b axis serves as the common axis being perpendicular to the basal plane of graphite, whereas the a and c axes are parallel to the surface but in various azimuthal angles relative to the direction of probe electrons, forming an ensemble average. Figure 2b shows the result from a 360° azimuthal

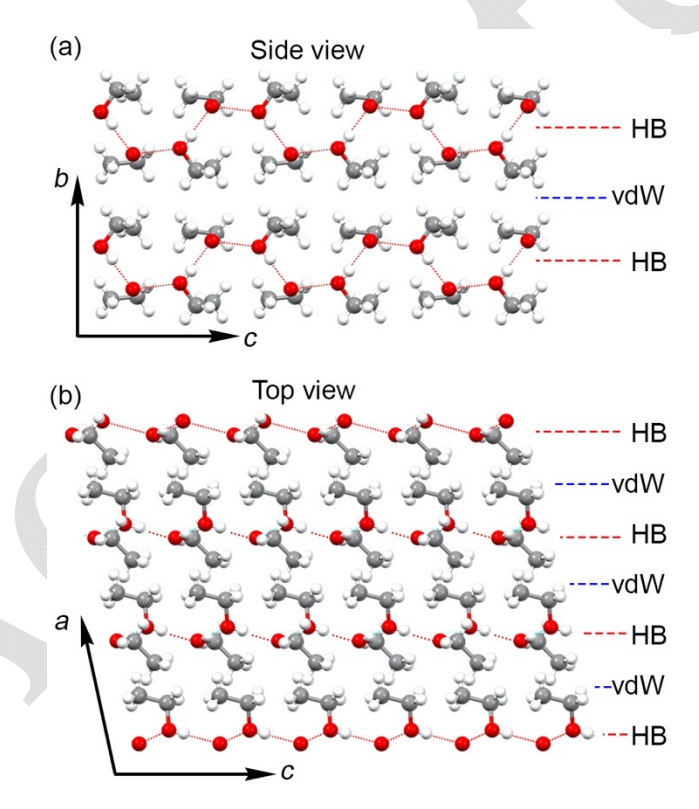


**Figure 3.** Structure of monoclinic solid ethanol. (a) Side view, with puckered (U-shaped) HB chains extending along *c*, being stacked along *b* and separated by regions of vdW forces. (b) Top view, with closer vdW contacts along *a* between HB chains. Carbon, oxygen, and hydrogen atoms are in gray, red, and white, respectively, and the hydrogen bonds are denoted by thin red lines.

average of the simulated patterns of a 2D crystalline slab with a thickness of one b unit cell, and Figure 2d shows that generated with a thickness of three b unit cells considering the observed increase in the vertical ordering (2.2 nm being close to 3\*b). The assignments of the Miller indices for the diffraction streaks, which are directly related to the in-plane 2D structure of solid ethanol, are also given.

Hence, we obtain the orientation information of crystallized multilayer films. Shown in Figure 3 is the monoclinic structure of solid ethanol, where the puckered (U-shaped) HB chains are along the *c* direction to form sheets in the *a*–*c* plane, stacked along the *b* direction and separated by the ethyl groups with van der Waals (vdW) interactions. Therefore, the appearance of many diffraction streaks (Figure 2, a and b) indicates the transition of an amorphous film to the organization of stacked in-plane 2D HB layers with a smooth surface, but without a well-defined vertical order concerning the sheets' azimuthal relations and interlayer spacing. The out-of-plane order and the resulting 3D ethanol crystallites are subsequently formed only in the small high temperature range when the HB molecules have enough mobility to move and readjust their orientations to complete the crystallization. Such a two-stage crystallization behavior is reminiscent of that of methanol deposited on smooth hydrophobic substrate surfaces, which also undergoes the transformations of the amorphous state to a stacking of 2D-layered HB sheets and then to 3D-ordered crystals during annealing.<sup>21</sup>

This behavioral similarity can be readily understood based on the common structural features of both molecular solids. At lower temperatures with less mobility, the stronger intermolecular hydrogen bonds cause the kinetic growth of the HB chains to lower the free energy, resulting in the formation of layers enclosing the hydrophilic parts and having the hydrophobic hydrocarbon groups on the outsides to interact with adjacent layers and with a

smooth hydrophobic surface including graphite. Hence, the presence of a substrate surface importantly helps inducing an order in these interfacial thin films, instead of random crystallite orientations, even when the vdW interaction per physisorbed small molecule may not be as strong as a chemical bond or Coulombic interaction serving as a guiding force in a chemisorption case.

However, notable differences between interfacial ethanol and methanol do exist. In a few rounds of depositions, we find that ethanol does not readily form as orderly stacked films on other smooth hydrophobic surfaces as on HOPG. After the vertical stacking order emerges on HOPG, the diffraction spots are never as sharp as those of 3D-ordered methanol,<sup>21</sup> which signifies the limited range of the layer alignment order in fully crystallized ethanol. Surprisingly, methanol does not form good layered films but instead randomly oriented crystallites on HOPG, as diffraction rings are observed from 10-nm methanol (Figure S1 in SI), unlike the situation on smooth hydrophobic surfaces.<sup>21</sup> These observations lead us to consider the role of HOPG's terraced topography for a template effect in the crystal growth. 18, 22, 24 Given the interlayer distance of 3.35 Å for graphite, the lattice constant of b = 6.882 Å for solid ethanol would mean a 1:2 layer ratio with a small tensile lattice mismatch of +2.7% for vdW-separated layers. The HB sheets grown on different steps may then be able to join and form a 2D-layered stacking (even with different azimuths) without large structural interruption. However, the good template condition may also imply difficulty to reorient the original azimuthally misaligned layers to form aligned 3D crystals, resulting in the aforementioned RHEED observation of a limited vertical order. In contrast, the lattice constant of c = 9.0403 Å for the methanol  $\alpha$  phase may have a 1:3 layer ratio with a large -10% mismatch, which would not be a favorable condition. As a result, the growth of HB chains of methanol molecules across neighboring steps may not maintain the

horizontal direction, eventually resulting in random orientations of crystallites on a terraced HOPG surface.

## 3.3 Near-commensurate interfacial structure of ethanol on graphene

The existence of an interfacial structure of ethanol physisorbed on graphite was reported previously using neutron and x-ray diffractions, although not in ultrahigh vacuum (Figure 4d). 45-46 In this commensurate structure, which may be designated as a 4×2 supercell, a = 9.84 Å is largely along the interchain direction, b = 4.92 Å is along the HB chain direction and is twice of graphene's unit-cell length, and the included angle is 60° (and hence a = 2b is 4 times of graphene's unit-cell length). The most prominent difference is the formation of zigzag (V-

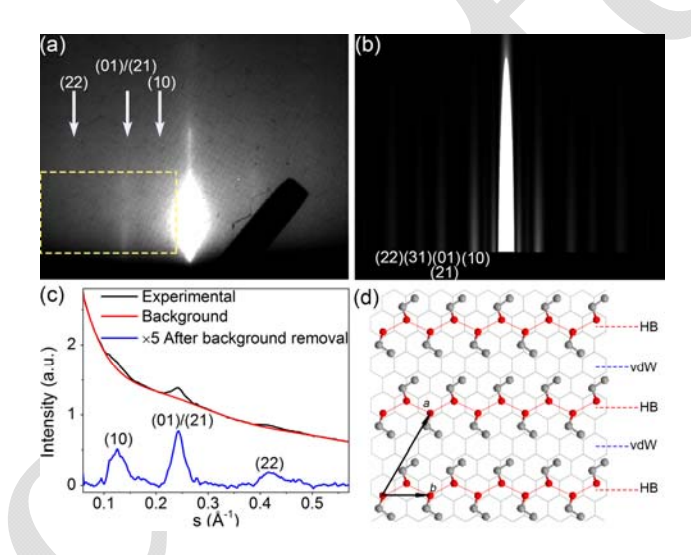


**Figure 4.** RHEED patterns and model of the interfacial structure of ethanol. (a) Diffraction of an ultrathin ethanol film with a nominal thickness of 0.4 nm, annealed up to 140 K. The yellow dashed rectangular region is used for intensity analysis. (b) Simulated pattern obtained using the model shown in (d). (c) Diffraction intensity curve (black) extracted from the horizontal strip indicated in (a), background profile obtained using a polynomial fit (red), and indexed diffraction peaks after subtraction of the background (blue). (d) Model of the near-commensurate  $4\times2$  interfacial ethanol structure with respect to the graphene lattice (light gray honeycomb). HB chains extend along b and are separated by interchain vdW regions along a (oxygen in red, carbon in dark gray, and hydrogen bonds in thin red lines; hydrogen atoms are omitted for clarity).

shaped) HB chains with nearly coplanar C-C-O bonds for all participating molecules, compared to the U-shaped HB chains with out-of-plane ethyl groups in the bulk. However, the recompressed exfoliated graphite used as the adsorbent has a very large mosaic spread angle of ~30°, high surface heterogeneity and discontinuity, small platelet sizes, impurity grains, and various sizes of pores. Thus, the use of a pure, more homogeneous graphite surface with a low mosaic spread angle is needed to re-examine the interfacial structures of various molecular assemblies.

Shown in Figure 4a is the RHEED image obtained from an ultrathin ethanol film with a nominal thickness of 0.4 nm annealed up to 140 K, which is close to or slightly higher than the coverage of one monolayer. A similar pattern is also observed for films with a nominal thickness of less than 1.5 nm (about two b unit cells of solid ethanol bulk), indicating the limited range for the influence of the HOPG surface on the annealed assembly structure. Clearly, the streak pattern is different from that of Figure 2a for the monoclinic structure. Three diffraction peaks can be identified after removal of the background fitted with a polynomial function (Figure 4c). The width of the clearest side streak is about 0.026 Å<sup>-1</sup>, which corresponds to ~3.7 nm for the average ordered domain size assuming a well-defined unit-cell length. This estimate may be only a lower bound if a small distribution of the unit-cell length exists and causes slightly varied peak positions and hence unavoidably an effective broader width.

Shown in Figure 4b is the kinematic scattering simulation result using a single layer of the structure in Figure 4d and an average of all in-plane azimuthal orientations, considering the ensemble measurement condition with the supporting HOPG substrate having grains of various azimuths. The positions of the experimentally observed diffraction peaks are largely reproduced with a minor adjustment (see below). The difference in the relative intensities is likely due to the

difference in order in the two unit-cell directions. The higher-than-expected (01) intensity corresponds well with a relative larger ordered range for the HB chain direction with the important intermolecular interactions to assemble ethanol molecules. The less-than-expected (10) and (31) intensities may reflect the limited ordered size for the interchain direction given the weaker vdW forces between chains and the same hexagonal symmetry for both graphene and the commensurate ethanol overlayer (Figure 4d). The HB chains grown from different nuclei may further exhibit directional turns by an integer multiple of 60°, resulting in a meandering assembly with less interchain order and hence decreased packing density. A similar idea may be found in a snapshot (although annealed at a much higher temperature) in a recent molecular dynamics study of 1-alcohols adsorbed on graphene.<sup>55</sup>

Furthermore, the HB O–O distances are equal (2.764 Å) with an O–O–O angle of 125.72° in the 4×2 commensurate overlayer structure, which is slightly longer than 2.716 Å and 2.730 Å with the O–O–O angles of 112.43° and 123.78° in the monoclinic bulk structure. <sup>51</sup> Hence, based on these structural differences, a relative tensile strain and hence free energy cost exist in the HB chains of the perfectly-commensurate interfacial structure, which may be relieved with an increasing distance from the substrate surface for weakened interfacial influence. This model is well supported by the position of the (01) streak of the interfacial structure as a function of nominal thickness (Figure 5). For perfect 4×2 commensuration, the momentum transfer (s) of the {01} $^{30}$  streak of HOPG at 0.469 Å<sup>-1</sup> (Figure 5a) should be double of that of the (01) streak of the ethanol overlayer, which is indicated by the black dashed line in Figure 5b. However, the experimental value of s of the (01) peak is larger, signifying that the commensuration may not be perfect and hence the ordered domain size is not very extended. As the ethanol film thickness increases from 0.2 to 1.5 nm, the s value of the (01) streak reaches that of the (02) one for

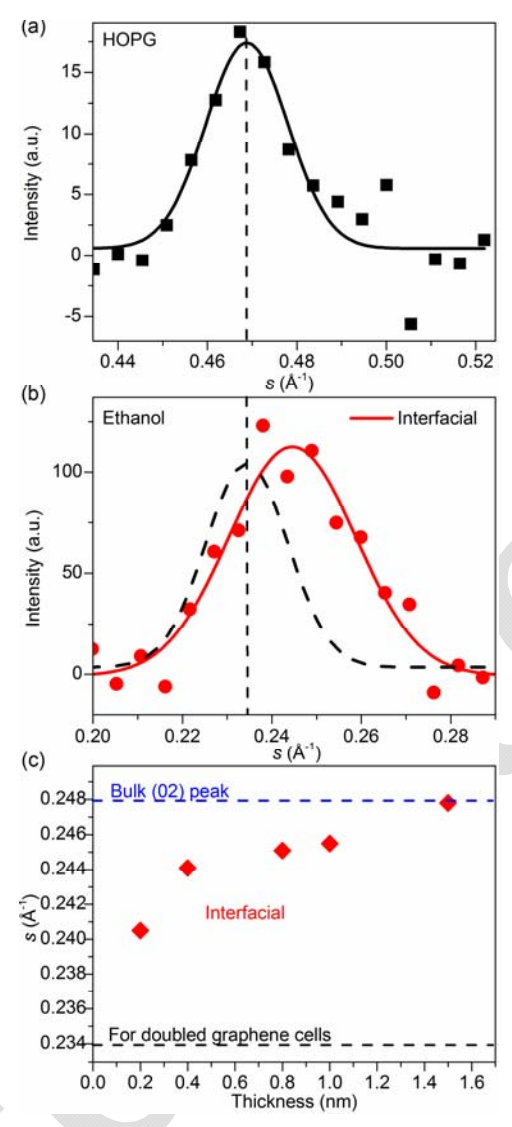
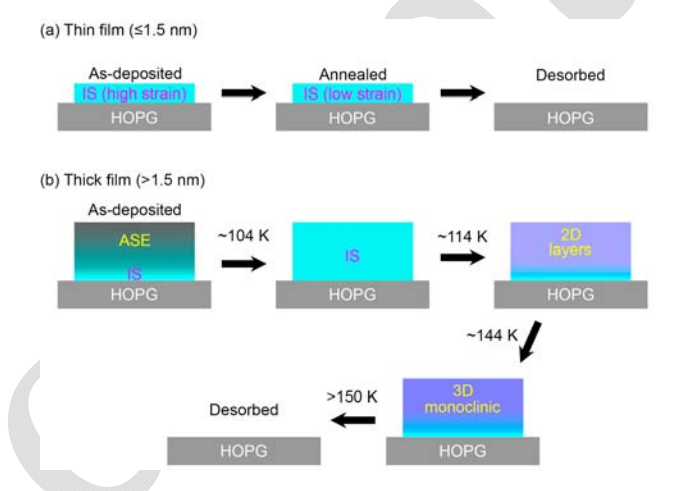


Figure 5. Diffraction peak positions and derived lattice strain of interfacial ethanol. (a) {10} diffraction peak of HOPG (black squares). The solid line is a Gaussian fit and the dashed line indicates the corresponding horizontal momentum transfer. (b) (01) diffraction peak of interfacial ethanol at 104–116 K (red dots; the red solid line is a Gaussian fit), compared to a hypothetical profile of HOPG with perfect commensuration (black dashed Gaussian curve). (c) Dependence of the position of the interfacial ethanol (01) peak on film thickness, measured at ~130 K. The deviation from the black dashed line (associated with perfect commensuration with the graphene lattice) indicates a small compressive lattice strain along the HB direction (related to the perfectly-commensurate structure). The approaching of the bulk monoclinic (02) peak in higher ethanol coverage signifies further relief of the strain and a transition from the interfacial region to the bulk-like structure.

monoclinic solid ethanol (Figure 5c), which indicates the trend for shorter O–O distances and therefore stronger hydrogen bonds away from the substrate. The matching of the *s* value also signifies the switch from the interfacial overlayer structure to the bulk at a nominal thickness of ~1.5 nm. We note that a very similar distance away from the HOPG surface has also been seen in a graphite–ionic liquid system for appearance of the bulk-like structure in deposited thin films.<sup>22</sup>

# 3.4 Ethanol on HOPG: Phase transitions and thickness dependence

With the aforementioned structural understanding, a schematic for the phase transitions of ethanol on HOPG can be reached, for two thickness ranges (Figure 6). Following its appearance upon deposition, the near-commensurate interfacial ethanol structure remains in ultrathin films with a nominal thickness of <1.5 nm, until the loss by molecular desorption at <140 K.



**Figure 6.** Schematics of the structures and phase-transition behavior of nanoscale ethanol films deposited on HOPG. (a) Presence of the near-commensurate interfacial structure (IS) of ethanol in as-deposited and annealed ultrathin films (with a nominal thickness up to 1.5 nm). The intrinsic lattice strain is gradually relieved during annealing. (b) Multi-stage structural transition in the upper part of ethanol films thicker than 1.5 nm, from as-deposited amorphous solid ethanol (ASE) to adoption of the interfacial structure beginning at ~104 K to stacked 2D layers without vertical ordering beginning at ~114 K to finally the 3D monoclinic crystalline structure before desorption at about 150 K. The near-commensurate interfacial structure remains in the interfacial region.

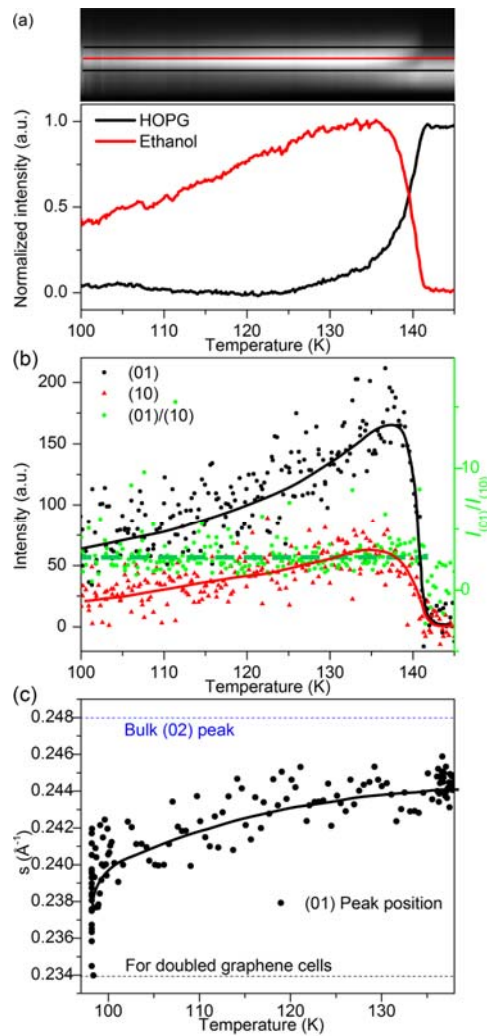


**Figure 7.** Diffraction intensities and peak positions of ultrathin ethanol films, with a nominal thickness of 0.4 nm, during the annealing. (a) Evolution of the center-streak vertical profile as a function of temperature (as the horizontal axis). The lower panel shows the intensities extracted along the red and black lines in the upper graph, which correspond to the diffractions of interfacial ethanol and HOPG, respectively. Because of the overlapped features, the HOPG intensity is calculated by subtracting the intensity at the upper black line from that at the lower black line to remove the ethanol contribution. (b) Evolution of the (01) and (10) side streak intensities of interfacial ethanol during annealing, with the solid lines as guides to the eye. The ratios of the two intensities are shown in green with a horizontal dashed line as a guide to the eye. (c) Evolution of the (01) peak position of interfacial ethanol film as a function of temperature, with the solid line as a guide to the eye. Accordingly, the lattice strain is not fully relieved even at the highest temperature possible, compared to that in a 1.5-nm film as shown in Figure 5c.

Diffraction intensity increases are observed during thermal annealing, signifying a growth period to form larger ordered domains [see Figure 7a for the center (00) streak and Figure 7b for the side (01) and (10) streaks; the ratios between these growing intensities remain largely constant as indicated by the green dots]. Concurrently, the *s* value of the interfacial ethanol (01) peak increases during annealing, which indicates a cell contraction along the HB direction (Figure 7c). Such a temperature-dependent observation of strain relief (Figure 6a) is again consistent with those thickness-dependent results discussed for Figure 5, b and c, showing the limited influence of the graphene surface relative to the thermal energy and interactions of ethanol molecules.

The phase-transition behavior in films thicker than 1.5 nm is quite complex, involving different assembly structures and their multi-stage interconversions (Figure 6b). At a substrate temperature lower than 100 K, an as-deposited film contains two parts, the interfacial structure near the substrate surface and an amorphous region away from the interface. The amorphous structure is formed because of the lack of significant interfacial guidance (Figure 1c). A gentle temperature increase by a few degrees allows the interfacial structure to affect the amorphous film and extend its range much farther away from the substrate surface (see Figure S2 for a typical RHEED image from the top of a 10-nm film in 104-114 K that resembles the patterns in Figure 1, b and d). However, a further increase of the temperature causes most of the film to convert to the bulk-like monoclinic structure, which implies, from the viewpoint of the energy landscape for a molecular assembly, a tilt of the balance between interfacial and intermolecular forces toward the latter at higher temperatures. The increase in molecular mobility in such a temperature range may have slightly reduced the strengths of both interfacial and intermolecular forces. However, it is the shift of the balance between the two that leads to the structural transformation (Figure 6b). It will be interesting to conduct studies using isothermal annealing and quantify the complex crystallization kinetics.<sup>56</sup> Previously, such a procedure was used on methanol thin films for the two-stage crystallization process, with much longer annealing times required for lower temperatures.<sup>21</sup> A similar behavior is found in ethanol thin films in preliminary experiments. This suggests that temperature is a major determining factor for phase transitions of molecular assemblies.

We note that different rates of intensity increase are seen for different diffraction streaks during the formation of the monoclinic structure (Figure 8a, middle light purple region). The (10) intensity, which is associated with the in-plane interchain direction formed with vdW forces, sees a clear delay and a slower rate in its increase compared to the (01) and (02) peaks associated with the HB direction. Thus, this result suggests a preference for the growth of HB chains followed by the chain packing during the formation of the 2D layers (Figure 3b); a mature film is reached at >125 K (Figure 8a). An aligned stacking of the 2D layers to form 3D-ordered crystals takes place only at an even higher temperature a few degrees prior to the film desorption (Figure 8a, dark purple region). By analyzing and separating the corresponding diffraction features, an estimate of the decreasing contribution by 2D ethanol layers and the increasing contributions by 3D ethanol crystals and the desorbed HOPG surface can be obtained (Figure 8b). The 2D-to-3D crystal growth goes on gradually and is still not completed after significant desorption begins. Such an observation is consistent with a previous report that a 3D single crystal could be grown at a temperature very close to the melting temperature.<sup>51</sup> As for the rise of the HOPG diffraction intensity, two desorption mechanisms are possible: in a layer-by-layer fashion keeping more uniform coverage or in patches producing island-like morphology. Either way allows more probing of the supporting surface, by penetrating a thinner ethanol film or by accessing an increasing area of exposed HOPG. From the analysis of the diffraction width we are not able to

reach a conclusion. Further investigation using isothermal annealing at a lower temperature with a slower desorption rate may be needed to determine the mechanism.

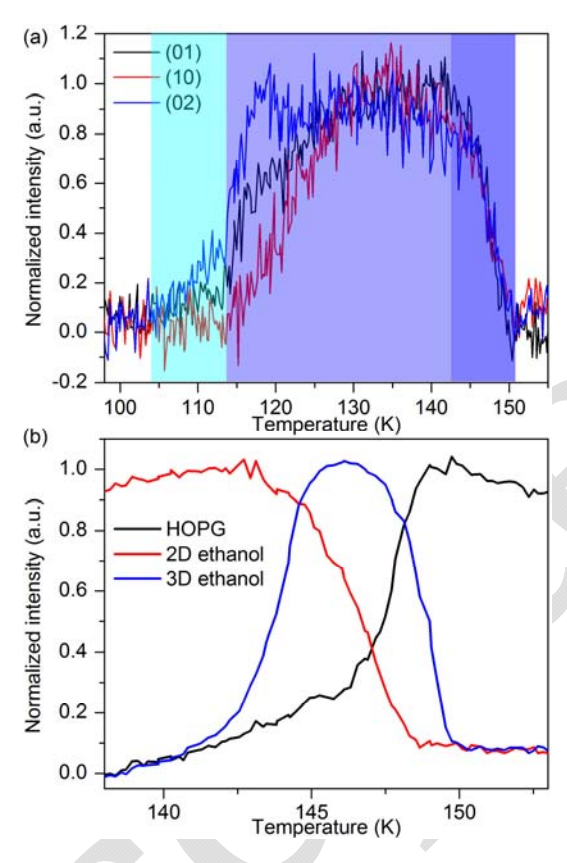


Figure 8. Diffraction intensities and structural contributions of multilayer ethanol films with a nominal thickness of 10 nm, during annealing and desorption. (a) Intensities of the side-streak regions related to the (01), (10), and (02) diffractions of bulk-like ethanol. The light blue, light purple, and dark purple regions specify the temperature ranges for the presence of the near-commensurate interfacial structure, stacked 2D layers, and 3D-ordered monoclinic crystallites, respectively. The decrease in intensity in the dark purple region signifies the loss of ethanol molecules due to concurrent desorption. (b) Diffraction intensities extracted from the center streak regions contributed by the HOPG, 2D-layered ethanol, and 3D-ordered ethanol structures. The structural conversion becomes accelerated in a temperature range similar to the onset of desorption, which implies the importance of increased molecular energy and mobility to the observed physical processes.

## 4. Conclusion

The ordered structures and unique phase-transition behavior of nanoscale ethanol films on

HOPG were studied using RHEED. The clear thickness- and temperature-dependent effects on the assembly structures in the temperature range between <100 K and 150 K, at an average ramping rate of 1.3 K/min, are the results of a delicate balance of the interfacial and intermolecular forces as well as the molecular energy. Because of the proximity to the HOPG surface, an interfacial structure is dominant in ultrathin films with a thickness of <1.5 nm, which is near-commensurate with a 4×2 supercell with respect to the graphene lattice at all temperatures until desorption. However, a lattice strain exists due to the slightly stretched hydrogen bonds, and therefore an increase in either the film thickness or the temperature can relieve the strain as a result of the diminished interfacial influence. For thicker films of 2 nm and above, the upper part above the interfacial ethanol structure undergoes multi-stage phase transitions, from an amorphous solid to adoption of the interfacial structure to a 2D-layered film to finally the monoclinic crystalline structure before desorption. Details of the crystallization kinetics signify the preference for an in-plain growth of the HB chains first, followed by the interchain vdW ordering. In addition, stacking of the 2D layers may be assisted by the terraced HOPG topography through a lattice-matching template effect. These rich structural forms and transformations of ethanol allow a closer look at the interplay between forces of different strengths near a substrate surface. Given the complex interfacial behavior, it is highly beneficial to use RHEED (and grazing incidence x-ray or neutron diffraction) as a direct structure-probing and non-contact method.

## **Supporting Information**

The Supporting Information is available free of charge.

RHEED images of a fully-annealed 10-nm-thick methanol thin film and a 10-nm-thick ethanol thin film annealed up to  $114~{\rm K}$ 

#### **AUTHOR INFORMATION**

## **Corresponding Author**

\*Email: <u>yang@uh.edu</u> Phone: +1 713-743-6022.

## **ORCID**

Xing He: 0000-0001-5341-5662

Ding-Shyue Yang: 0000-0003-2713-9128

## **Notes**

The authors declare no competing financial interest.

## **ACKNOWLEDGEMENTS**

This research was supported by a National Science Foundation CAREER Award (CHE-1653903) and the R. A. Welch Foundation (E-1860).

## REFERENCES

- 1. Fedorov, M. V.; Kornyshev, A. A., Ionic liquids at electrified interfaces. *Chem. Rev.* **2014**, *114*, 2978-3036.
- 2. Baldelli, S., Surface structure at the ionic liquid–electrified metal interface. *Acc. Chem. Res.* **2008**, *41*, 421-431.
- 3. Silvester, D. S.; Jamil, R.; Doblinger, S.; Zhang, Y.; Atkin, R.; Li, H., Electrical double layer structure in ionic liquids and its importance for supercapacitor, battery, sensing, and lubrication applications. *J. Phys. Chem. C* **2021**, *125*, 13707-13720.
- 4. An, S. J.; Li, J.; Daniel, C.; Mohanty, D.; Nagpure, S.; Wood, D. L., The state of understanding of the lithium-ion-battery graphite solid electrolyte interphase (SEI) and its relationship to formation cycling. *Carbon* **2016**, *105*, 52-76.
- 5. Yang, C.; Hu, C.; Xiang, C.; Nie, H.; Gu, X.; Xie, L.; He, J.; Zhang, W.; Yu, Z.; Luo, J., Interfacial superstructures and chemical bonding transitions at metal-ceramic interfaces. *Sci. Adv.* **2021**, *7*, eabf6667.
- 6. Liu, H.; Song, C.; Zhang, L.; Zhang, J.; Wang, H.; Wilkinson, D. P., A review of anode catalysis in the direct methanol fuel cell. *J. Power Sources* **2006**, *155*, 95-110.
- 7. Luneau, M.; Lim, J. S.; Patel, D. A.; Sykes, E. C. H.; Friend, C. M.; Sautet, P., Guidelines to achieving high selectivity for the hydrogenation of α,β-unsaturated aldehydes with bimetallic

- and dilute alloy catalysts: a review. Chem. Rev. 2020, 120, 12834-12872.
- 8. Kakaei, K.; Esrafili, M. D.; Ehsani, A., Alcohol oxidation and hydrogen evolution. In *Interface Science and Technology*, Kakaei, K.; Esrafili, M. D.; Ehsani, A., Eds. Elsevier: Amsterdam, The Netherlands, 2019; Vol. 27, pp 253-301.
- 9. Zhang, X.; Coleman, A. C.; Katsonis, N.; Browne, W. R.; van Wees, B. J.; Feringa, B. L., Dispersion of graphene in ethanol using a simple solvent exchange method. *Chem. Commun.* **2010**, *46*, 7539-7541.
- 10. Robertson, E. J.; Olivier, G. K.; Qian, M.; Proulx, C.; Zuckermann, R. N.; Richmond, G. L., Assembly and molecular order of two-dimensional peptoid nanosheets through the oil–water interface. *Proc. Natl. Acad. Sci. U.S.A.* **2014**, *111*, 13284-13289.
- 11. Wang, Y.; Papanikolaou, K. G.; Hannagan, R. T.; Patel, D. A.; Balema, T. A.; Cramer, L. A.; Kress, P. L.; Stamatakis, M.; Sykes, E. C. H., Surface facet dependence of competing alloying mechanisms. *J. Chem. Phys.* **2020**, *153*, 244702.
- 12. He, J.; Toriello, F. E.; Emtiaz, S. M.; Henning, T.; Vidali, G., Phase transition of interstellar CO ice. *Astrophys. J. Lett.* **2021**, *915*, L23.
- 13. Shiotari, A.; Sugimoto, Y., Ultrahigh-resolution imaging of water networks by atomic force microscopy. *Nat. Commun.* **2017**, *8*, 14313.
- 14. McQuillan, N. M.; Larson, A. M.; Sykes, E. C. H., Low-cost spectrum analyzer for trouble shooting noise sources in scanning probe microscopy. *J. Vac. Sci. Technol* **2020**, *38*, 061202.
- 15. Burke, D. J.; Wolff, A. J.; Edridge, J. L.; Brown, W. A., The adsorption and desorption of ethanol ices from a model grain surface. *J. Chem. Phys.* **2008**, *128*, 104702.
- 16. Tylinski, M.; Smith, R. S.; Kay, B. D., Structure and desorption kinetics of acetonitrile thin films on Pt(111) and on graphene on Pt(111). *J. Phys. Chem. C* **2020**, *124*, 2521-2530.
- 17. Tylinski, M.; Smith, R. S.; Kay, B. D., Morphology of vapor-deposited acetonitrile films. *J. Phys. Chem. A* **2020**, *124*, 6237-6245.
- 18. Yang, D.-S.; Zewail, A. H., Ordered water structure at hydrophobic graphite interfaces observed by 4D, ultrafast electron crystallography. *Proc. Natl. Acad. Sci. U.S.A.* **2009**, *106*, 4122-4126.
- 19. Scherzer, M.; Girgsdies, F.; Stotz, E.; Willinger, M.-G.; Frei, E.; Schlögl, R.; Pietsch, U.; Lunkenbein, T., Electrochemical surface oxidation of copper studied by in situ grazing incidence X-ray diffraction. *J. Phys. Chem. C* **2019**, *123*, 13253-13262.

- 20. Wannapaiboon, S.; Schneemann, A.; Hante, I.; Tu, M.; Epp, K.; Semrau, A. L.; Sternemann, C.; Paulus, M.; Baxter, S. J.; Kieslich, G., et al., Control of structural flexibility of layered-pillared metal-organic frameworks anchored at surfaces. *Nat. Commun.* **2019**, *10*, 346.
- 21. He, X.; Wu, C.; Yang, D.-S., Communication: no guidance needed: ordered structures and transformations of thin methanol ice on hydrophobic surfaces. *J. Chem. Phys.* **2016**, *145*, 171102.
- 22. He, X.; Wu, C.; Rajagopal, K.; Punpongjareorn, N.; Yang, D.-S., Ordered ionic liquid structure observed at terraced graphite interfaces. *Phys. Chem. Chem. Phys.* **2016**, *18*, 3392-3396.
- 23. Souda, R.; Aizawa, T., Wettability of bare and graphene-adsorbed Pt(111) during glass–liquid transition, crystallization, and premelting of water. *J. Phys. Chem. C* **2018**, *122*, 28094-28104.
- 24. Wu, C.; Yang, D.-S., Ordered structures and morphology-induced phase transitions at graphite–acetonitrile interfaces. *J. Phys. Chem. C* **2019**, *123*, 22390-22396.
- 25. Ghosh, M.; Yang, D.-S., Structures of self-assembled *n*-alkanethiols on gold by reflection high-energy electron diffraction. *Phys. Chem. Chem. Phys.* **2020**, *22*, 17325-17335.
- 26. Ghosh, M.; Yang, D.-S., Ordering of small molecules on hydrophobic self-assembled *n*-alkanethiols: delicate balance of interfacial and intermolecular interactions. *J Phys. Chem. C* **2021**, *125*, 19022-19031.
- 27. Souda, R.; Aizawa, T., Crystallization kinetics of water on graphite. *Phys. Chem. Chem. Phys.* **2018**, *20*, 21856-21863.
- 28. Souda, R.; Aizawa, T., Crystallization kinetics of thin water films on Pt(111): effects of oxygen and carbon-monoxide adspecies. *Phys. Chem. Chem. Phys.* **2019**, *21*, 1123-1130.
- 29. Souda, R.; Aizawa, T., Nucleation and growth of water ice on oxide surfaces: the influence of a precursor to water dissociation. *Phys. Chem. Chem. Phys.* **2020**, *22*, 20515-20523.
- 30. Souda, R.; Aizawa, T., Crystallization kinetics of water on bare, hydrogenated, and hydroxylated Si(100) and Si(111) surfaces studied by RHEED, TOF-SIMS, and TPD. *J. Phys. Chem. C* **2019**, *123*, 20373-20383.
- 31. Jones, A. O. F.; Chattopadhyay, B.; Geerts, Y. H.; Resel, R., Substrate-induced and thin-film phases: polymorphism of organic materials on surfaces. *Adv. Funct. Mater.* **2016**, *26*, 2233-2255.

- 32. Nie, X.; Ma, F.; Ma, D.; Xu, K., Thermodynamics and kinetic behaviors of thickness-dependent crystallization in high-k thin films deposited by atomic layer deposition. *J. Vac. Sci. Technol. A* **2015**, *33*, 01A140.
- 33. Zondlo, M. A.; Onasch, T. B.; Warshawsky, M. S.; Tolbert, M. A.; Mallick, G.; Arentz, P.; Robinson, M. S., Experimental studies of vapor-deposited water—ice films using grazing-angle FTIR-reflection absorption spectroscopy. *J. Phys. Chem. B* **1997**, *101*, 10887-10895.
- 34. Pratontep, S.; Brinkmann, M.; Nüesch, F.; Zuppiroli, L., Nucleation and growth of ultrathin pentacene films on silicon dioxide: effect of deposition rate and substrate temperature. *Synth. Met.* **2004**, *146*, 387-391.
- 35. Andersson, P. U.; Suter, M. T.; Marković, N.; Pettersson, J. B. C., Water condensation on graphite studied by elastic helium scattering and molecular dynamics simulations. *J Phys. Chem. C* **2007**, *111*, 15258-15266.
- 36. Hooks, D. E.; Fritz, T.; Ward, M. D., Epitaxy and molecular organization on solid substrates. *Adv. Mater.* **2001**, *13*, 227-241.
- 37. Wang, L.; King, I.; Chen, P.; Bates, M.; Lunt, R. R., Epitaxial and quasiepitaxial growth of halide perovskites: new routes to high end optoelectronics. *APL Mater.* **2020**, *8*, 100904.
- 38. Rietzler, F.; Nagengast, J.; Steinrück, H. P.; Maier, F., Interface of ionic liquids and carbon: ultrathin [C<sub>1</sub>C<sub>1</sub>Im][Tf<sub>2</sub>N] films on graphite and graphene. *J. Phys. Chem. C* **2015**, *119*, 28068-28076.
- 39. Sitaputra, W.; Stacchiola, D.; Wishart, J. F.; Wang, F.; Sadowski, J. T., In situ probing of ion ordering at an electrified ionic liquid/Au interface. *Adv. Mater.* **2017**, *29*, 1606357.
- 40. Fayos, R.; Bermejo, F. J.; Dawidowski, J.; Fischer, H. E.; González, M. A., Direct experimental evidence of the relationship between intermediate-range order in topologically disordered matter and discernible features in the static structure factor. *Phys. Rev. Lett.* **1996**, 77, 3823-3826.
- 41. Srinivasan, A.; Bermejo, F. J.; de Andrés, A.; Dawidowski, J.; Zúñiga, J.; Criado, A., Evidence for a supercooled plastic-crystal phase in solid ethanol. *Phys. Rev. B* **1996**, *53*, 8172-8175.
- 42. Talón, C.; Ramos, M. A.; Vieira, S.; Cuello, G. J.; Bermejo, F. J.; Criado, A.; Senent, M. L.; Bennington, S. M.; Fischer, H. E.; Schober, H., Low-temperature specific heat and glassy dynamics of a polymorphic molecular solid. *Phys. Rev. B* **1998**, *58*, 745-755.

- 43. Efimov, V.; Izotov, A.; Rybchenko, O., Dynamics of crystallization of solid ethanol. *Low Temp. Phys.* **2018**, *44*, 1105-1110.
- 44. Liriano, M. L.; Larson, A. M.; Gattinoni, C.; Carrasco, J.; Baber, A. E.; Lewis, E. A.; Murphy, C. J.; Lawton, T. J.; Marcinkowski, M. D.; Therrien, A. J., et al., Chirality at two-dimensional surfaces: a perspective from small molecule alcohol assembly on Au(111). *J. Chem. Phys.* **2018**, *149*, 034703.
- 45. Herwig, K. W.; Trouw, F. R., Ethanol on graphite: the influence of hydrogen bonding on surface melting. *Phys. Rev. Lett.* **1992**, *69*, 89-92.
- 46. Morishige, K., Structure and melting of a monolayer ethanol film on graphite. *J. Chem. Phys.* **1992**, *97*, 2084-2089.
- 47. Ichimiya, A.; Cohen, P. I., *Reflection High-Energy Electron Diffraction*; Cambridge University Press: Cambridge, 2004.
- 48. Eaglesham, D. J.; Cerullo, M., Dislocation-free Stranski-Krastanow growth of Ge on Si(100). *Phys. Rev. Lett.* **1990**, *64*, 1943-1946.
- 49. Liu, X.; Han, Y.; Evans, J. W.; Engstfeld, A. K.; Behm, R. J.; Tringides, M. C.; Hupalo, M.; Lin, H.-Q.; Huang, L.; Ho, K.-M., et al., Growth morphology and properties of metals on graphene. *Prog. Surf. Sci.* **2015**, *90*, 397-443.
- 50. Warren, B. E., X-ray Diffraction; Dover Publications: New York, 1990.
- 51. Jönsson, P. G., Hydrogen bond studies. CXIII. The crystal structure of ethanol at 87 K. *Acta Cryst. B* **1976**, *32*, 232-235.
- 52. Morishige, K.; Kawamura, K.; Yamamoto, M.; Ohfuji, I., Capillary condensation of xenon on exfoliated graphite. *Langmuir* **1990**, *6*, 1417-1421.
- 53. Takayoshi, S.; Fukuyama, H., Determination of the mosaic angle distribution of grafoil platelets using continuous-wave NMR spectra. *J. Low Temp. Phys.* **2009**, *158*, 672.
- 54. Morishita, M., Surface observation and magnetization measurements of grafoil substrate. *J. Low Temp. Phys.* **2011**, *162*, 638-644.
- 55. Zangi, R., Self-assembly of alcohols adsorbed on graphene. *J. Phys. Chem. C* **2019**, *123*, 16902-16910.
- 56. Smith, R. S.; Tylinski, M.; Kimmel, G. A.; Kay, B. D., Crystallization kinetics of amorphous acetonitrile nanoscale films. *J. Chem. Phys.* **2021**, *154*, 144703.